

## Supporting Information

### Light-driven ultrafast sensor based on biocompatible solvatochromic metal-organic framework

Maria Timofeeva,<sup>a†</sup> Yuliya Kenzhebayaeva,<sup>a†</sup> Nikita Burzak,<sup>b†</sup> Agniia Bazhenova,<sup>c</sup> Artem Lunev,<sup>a</sup> Alexander S. Novikov,<sup>d,e</sup> Andrey B. Bondarenko,<sup>b,f</sup> Sergei A. Shipilovskikh,<sup>a\*</sup> Vyasheslav A. Dyachuk,<sup>g\*</sup> Valentin A. Milichko,<sup>a,h\*</sup>

### Materials and Methods

*Chemicals.* All materials including  $\text{CoCl}_2 \cdot 6\text{H}_2\text{O}$  (Sigma-Aldrich,  $\geq 99.0\%$ ),  $\text{CoSO}_4 \cdot 7\text{H}_2\text{O}$  (Sigma-Aldrich,  $\geq 99.0\%$ ),  $\text{NiCl}_2 \cdot 6\text{H}_2\text{O}$  (Sigma-Aldrich,  $\geq 99.0\%$ ),  $\text{CuCl}_2 \cdot 2\text{H}_2\text{O}$  (Sigma-Aldrich,  $\geq 99.0\%$ ), 1,3,5-benzenetricarboxylic acid (Sigma-Aldrich, Trimesic acid ( $\text{H}_3\text{BTC}$ ), 95%), dimethylformamide (ACS reagent,  $\geq 99.8\%$ ), and ethanol (ACS reagent,  $\geq 99.5\%$ ) were used in all syntheses.

*Synthesis of MOF microcrystals and powder.*  $\text{CoCl}_2 \cdot 6\text{H}_2\text{O}$  (40 mg, 0.168 mmol) was dissolved in mixture of solvents 1 ml N,N'-dimethylformamide (DMF) and 1 ml ethanol (EtOH), then placed into a beaker. Then vial was immersed in an ultrasonic bath for 10 min. In another beaker the solution of trimesic acid ( $\text{H}_3\text{BTC}$ ) (18 mg, 0.084 mmol) in 1 ml of  $\text{H}_2\text{O}$  was prepared. After the solution mixture was placed into 4 ml vial and hermetically sealed with a lid with a rubber septum to exclude the interaction with the external environment and create excess pressure in the vessel. The solution mixture was heated to 80 °C and kept for 48 h. After 48 h the reaction mixture was cooled down to room temperature. The resulting powder was separated from the mother liquid by filtration, then it was repeatedly washed 5 times with a mixture of DMF/EtOH/ $\text{H}_2\text{O}$ . The washed powder was dried in the air. A pink homogeneous powder was obtained. Similarly, the crystal of the MOFs was obtained except for the absence of mixing of the reaction medium during the synthesis, as this promotes the growth of crystals. Similarly, the MOFs based on  $\text{CoSO}_4 \cdot 7\text{H}_2\text{O}$ ,  $\text{NiCl}_2 \cdot 6\text{H}_2\text{O}$  and  $\text{CuCl}_2 \cdot 2\text{H}_2\text{O}$  salts were also obtained (see PXRD and CCDC data in Figs. S17a, S18a, S19a).

*Single crystal X-ray diffraction.* The SCXRD analysis was performed on Kappa single Xcalibur and Oxford Diffraction Sapphire3 Gemini S diffractometers from Rigaku XtaLAB Pro.

*Powder X-ray diffraction.* The PXRD patterns were recorded on a Shimadzu 7000-maxima X-ray diffractometer with a 2 kW characteristic  $\text{CuK}\alpha$  ( $\text{K}\alpha 1 \lambda = 1.54059 \text{ \AA}$ , angular range  $2\theta = 5^\circ - 80^\circ$ ) X-ray radiation source and a Bragg-Brentano goniometer geometry. The angular resolution during the analysis was 0.01 degree at a scanning speed of 0.7 degrees  $\text{min}^{-1}$ . Also, for the analysis of the

crystalline structure of the powder of MOFs (Figures S17-S19, and S21), an Ultima IV X-ray diffractometer (Rigaku, Japan) was used. The radiation wavelength of the copper anode is  $\text{CuK}\alpha = 1.5418 \text{ \AA}$ . Measurements were performed in the range of 5-50 degrees with a step of measurement 0.02 degrees, and the measurement speed was 0.5 degrees per min.

*XRD data processing.* Calculation used the GSAS-II software, an open-source software developed by the Argonne National Laboratory for the refinement of crystallographic structure models. Experimental input was generated by the Rigaku SmartLab X-Ray diffraction system. The system used a Cu target ( $\text{K}\alpha_1$  1.540593,  $\text{K}\alpha_2 = 1.544414$ ) with a nickel-based beta-filter and a focal spot size of  $0.4 \text{ mm} \times 12 \text{ mm}$  in the Bragg-Brentano geometry. Data processing was carried out by applying multi-stage optimization permitted by the GSAS-II software. This helped reducing the possible effect of parameter collinearity during optimisation and decreased the chances of getting abnormal parameter values. The background was determined using a Chebyshev polynomial (6<sup>th</sup> to 8<sup>th</sup> order) with one additional amorphous peak initially assumed at  $2\theta = 23^\circ$  and subsequently optimised. A variable sample displacement was introduced, with a typical value below  $100 \text{ }\mu\text{m}$ . The XRD pattern was simulated using the structure recorded in a CIF file. After partial optimisation of the background coefficients and the sample displacement, the monoclinic unit cell parameters ( $a$ ,  $b$ ,  $c$  and  $\beta$ ) were optimized. Subsequently, the crystallite size and isotropic microstrain were refined. To correctly account for instrumental broadening, the discrepancy between the calculated profile and the input data was used to calibrate the instrumental parameters while assuming the material was single-phase and correctly described by the input CIF file. To make sure calibration was performed correctly, the peak widths were checked to always stay positive.

Two calculations were performed for each profile (Figures S2-S4): with and without optimizing the relative atomic positions in the unit cell. Since the input number of atoms characteristic to the MOF structure was large, all their positions could not be optimized simultaneously due to parameter collinearity. This was especially complicated by the noise in the measurement data collected on the experimental samples. Regardless, it was possible to optimize just the equilibrium positions of the metal atoms and their nearest neighbors.

*Scanning electron microscopy.* The chemical composition and homogeneity of obtained MOFs were controlled with SEM (Quanta 200, FEI, Netherlands) with an acceleration voltage of 10 kV. The dried MOFs were coated with a gold thin film for imaging with SEM.

*BET analysis.*  $\text{N}_2$  sorption-desorption data along with surface area analysis and pore size were analyzed with the surface area and pore size analyzer Quantachrome NOVA 1200e (Figure S16). Before each test, the sample was degassed at  $250 \text{ }^\circ\text{C}$  for 16 h. The specific surface area of the samples and the pore distribution were calculated by applying the DFT.

*Colorimetric selectivity.* The powder of the MOFs and salts (Figure 3a, S17b, S18b, S19b, and S20) was prepared on a polymer substrate. Drops of different solvents were applied alternately to the powder by a Pasteur pipette. After each exposure, the powder was dried on a tile to get rid of solvent.

*Video analysis.* The process of color change was visually detected on the CCD camera of the mobile phone at a frequency of 120 frames per second (Video S1, S2). The time of color change was extracted from the resulting storyboard.

*Raman spectroscopy.* Raman analysis was performed using self-made confocal optical setup based on HORIBA LabRam spectrometer with a water-cooling charge-coupled device (CCD, Andor DU 420A-OE 325) with a  $600\text{ g mm}^{-1}$  and  $1800\text{ g mm}^{-1}$  diffraction gratings and high aperture objective (Mitutoyo Plan Apo, 100x VIS, 0.9 NA) moving with Thorlabs piezo-stage. Raman scattering signal was measured under excitation by a 632.8 nm He-Ne continuous laser radiation in reflection mode (Figures 2a, S8).

*Transmittance spectroscopy.* The transmittance spectra of single crystals of MOFs (Figure 2b, Figure S6) were measured in air with the help of self-made confocal microscope setup. The MOF crystals were radiated by white halogen lamp (Avantes) of 360-2500 nm range. The light was focused on the sample with an objective (Mitutoyo HR NIR 10x, 0.26 NA) while the transmitted signal was collected by an objective (Mitutoyo 50x, 0.55 NA). The collected signal was analyzed by HORIBA LabRAM confocal spectrometer with a water cooling charge-coupled device (CCD, Andor DU 420A-OE 325) with a  $150\text{ g mm}^{-1}$  diffraction grating.

*Infra-red laser heating.* In order to demonstrate the effect of color change acceleration by infra-red laser heating, the single crystal of MOF **2** was moistened in DMF. As a radiation source, a white halogen lamp of 360–2500 range (Avantes) was used. We focused the light from the halogen lamp on the single crystals with an objective (Mitutoyo HR NIR 10x, 0.26 NA). To observe the change of color upon the laser irradiation, the 1050 nm wavelength (80 MHz repetition rate, 150 fs pulse duration, 5 mW integral power) laser pulses have been focused on the MOF through an objective (Mitutoyo HR NIR 10x, 0.28 NA). Through the laser radiation motion, the local color change was observed (Figure S6).

*Fish husbandry, embryo collection, adult fish and embryo exposure.* Adult zebrafish were raised according to standard breeding protocols (temperature 28 °C, photoperiod 14/10 h day/night) in ZebTec Aquatic recirculation system (Tecniplast, Italy) located in Preclinical Translational Research Centre of Almazov National Medical Research Centre. Filtered water, passed through a system of reverse osmosis (pH 7.0), was supplied to the recirculation system with conductivity about 800-840 S  $\text{cm}^{-1}$ . Adult zebrafish were fed twice a day in the form of dry fish food (TetraMin Flakes, Tetra GmbH, Germany) and live artemia nauplii (Barrom, Barnaul, Russia).

The behavioral response of zebrafish was assessed using transparent behavioral chambers, 20x20x5 cm in size. The development status of zebrafish embryos was observed with stereomicroscope Zeiss Stereo Discovery v12 (Zeiss, Germany). The embryos used for chemical treatment were obtained by spawning adult fish in spawning tanks (Tecniplast, Italy) overnight with males and females in a 2:2 ratio.

We adhered to the general guidelines, in agreement with EU Directive 2010/63/EU for animals, for zebrafish handling, mating, embryo collection and maintenance. Approval for this study was provided by the local committee on the Ethics of Animal Experiments (Almazov Centre; Permit Number: П3\_23\_12\_Dyachuk VA).

*Adult zebrafish behavior and mortality assay.* To assess the toxicity, we used 4 groups of experimental animals with 6 individuals each, the age of the zebrafish was 6 months, the average weight was 330 mg. Each group of zebrafish was given 20  $\mu$ l of a suspension of MOFs of different concentrations intragastrically. Suspensions were prepared in the E3 medium at four concentrations (200, 100, 50, and 25 g L<sup>-1</sup>). These volumes corresponded to dosages of 12, 6, 3, and 1.5 g kg<sup>-1</sup> of fish weight. To introduce the suspension into the stomach, we immobilized the fish by incubating them in a 170 mg l<sup>-1</sup> tricaine solution for 5 min, after MOFs injection we placed the fish in an aquarium with running water. Adult zebrafish mortality as toxicity endpoint was assessed after the introduction of the suspension into the stomach after 6 h. At this time interval, a behavioral test was conducted, and we assessed the distribution of fish in behavioral chambers. The toxic effect on fish behavior included anxiety, depressed behavior, and the position the fish occupied in the aquarium (Figure 3b,c).

*Zebrafish embryo mortality assay.* Fertilized eggs were collected within 1 h after the light switched on and rinsed in E3 medium, then normal embryos were inspected, staged and dechorionized after 48 hpf (hours post fertilization) for the following experiment under a stereomicroscope. Embryos were exposed to different concentrations (10.00, 5.00, 2.50, 1.25, 0.63, 0.32, 0.16, 0.08, 0.04, and 0.00 g l<sup>-1</sup>) of MOF for two periods: 24 and 48 h. We determined embryo mortality by heartbeat and blood flow using an inverted microscope (Zeiss, Germany). We recorded the results in 24 and 48 h after placing 48 dpf embryos in wells of a plate with MOFs. During the experiment, we incubated the embryos in a thermostat at 28 °C. Each concentration of the drug at which toxicity was studied corresponded to six repetitions.

*Cell culture.* The human glioblastoma multiform tumor T98G cell line was purchased from the Institute of Cytology, Russian Academy of Sciences (Saint Petersburg, Russia). Cells were maintained in Dulbecco's Modified Eagle Medium (DMEM) (Biolot, Russia); supplemented with 100 IU mL<sup>-1</sup> penicillin, 0.1 mg mL<sup>-1</sup> streptomycin (Biolot, Russia), and 10 % Fetal Calf Serum (FCS) (Neofroxx, Germany) at 37 °C in a humidified atmosphere containing 5 % CO<sub>2</sub>. Having

reached confluence (> 90 %), cells were detached with 0.25 % trypsin, 0.53 mM EDTA solution (ethylenediaminetetraacetic acid, Biolut, Russia) for 2 min and seeded to attach at a density of  $40.0 \times 10^3$  cells  $\text{cm}^{-2}$  in 96-well or 24-well plates according to the specific experiment.

*Cell viability assay of MOFs (MTT assay).* To determine the viability of T98G cells, the MTT (3-[4,5-dimethylthiazol-2yl]-2,5-diphenyltetrazolium bromide) colorimetric assay was performed. The MTT assay involves the conversion of the water-soluble yellow dye MTT to an insoluble purple formazan by the action of mitochondrial reductase in living cells. T98G cells were seeded in 96-well plates in 100  $\mu\text{L}$  of culture media and incubated for 24 h at 37 °C with 5 %  $\text{CO}_2$  to allow for cell adhesion. Then cells were exposed to different concentrations of the MOF suspension (0–2000  $\mu\text{g mL}^{-1}$ ) with six biological replicates for each concentration for 6, 18 or 24 h at 37 °C with 5 %  $\text{CO}_2$ . After the indicated period of incubation 10  $\mu\text{L}$  of 12 mM MTT solution in PBS (5 mg  $\text{mL}^{-1}$ , Cat #1334GR001, Neofroxx, Germany) were added to each well and incubated for two hours at 37 °C with 5 %  $\text{CO}_2$ . Then the culture media with MTT solution was discarded and 100  $\mu\text{L}$  of SDS (Sodium dodecyl sulfate) - HCl (10 % (m  $\text{v}^{-1}$ ) SDS in 0.01N HCl) solution were added to each well to dissolve the formed formazan dye, and then the microplate was incubated for 3 h at 37 °C in a humidified chamber. Finally, the absorbance in each well was measured with Multiskan™ SkyHigh microplate reader (Thermo Fisher Scientific Inc.; Waltham, MA, USA) at 570 nm. The percentage viability (in %), which is proportional to metabolic active cell number, converting MTT to formazan dye, was calculated as follows: % Viability = OD in test well/OD in control well  $\times$  100.

*Cellular exposure to MOFs.* T98G cells were seeded on 12 mm round glass coverslips (MiniMed, Russia) in the wells of 24-well culture plates and were incubated at 37 °C in a 5 %  $\text{CO}_2$  atmosphere for 24 h. The cell culture medium then was removed and 1 mL of fresh complete medium containing appropriate concentrations (0  $\mu\text{g mL}^{-1}$ , 31.25  $\mu\text{g mL}^{-1}$ , 250  $\mu\text{g mL}^{-1}$ , and 1000  $\mu\text{g mL}^{-1}$ ) of dispersed MOFs or 2 mM DTT (dithiothreitol) as a positive control (apoptosis induction) was added to each well and incubated for 6, 18, and 24 h. At each of three time points after the MOF treatment the cells were washed with phosphate-buffered saline (PBS) and fixed with 4 % paraformaldehyde in PBS for 15 min. Then the cells were permeabilized with 0.5 % PBS-buffered Tween-20 (Sigma-Aldrich, France) for 15 min, and stained for apoptosis (Caspase3 or TUNEL assay) and cell proliferation (Ki67) evaluation.

*Immunofluorescent detection of active Caspase-3.* To detect the apoptotic cells by immunocytochemistry rabbit polyclonal anti-Cleaved Caspase-3 (Asp175) antibodies (1:400 dilution, Cat #9661, Cell Signaling Technology, Danvers, MA, USA) were used. After permeabilization, T98G cells on coverslips were washed three times with PBS for 5 min each and incubated with anti-Cleaved Caspase-3 antibodies and Alexa Fluor 555 Phalloidin (1:500 dilution,

Cat #A34055, Thermo Fisher Scientific, Waltham, MA, USA) in blocking serum solution (5 % normal donkey serum in 1× PBS/ 0.5 % Tween-20) overnight at 4 °C. After incubation cells were washed with PBST (0.5 % PBS-buffered Tween-20) for 5 min twice, the secondary donkey anti-rabbit Alexa Fluor 647 antibodies (1:500 dilution, Cat #A-31573, Thermo Fisher Scientific, Waltham, MA, USA) were added and incubated at room temperature for 1h. Afterwards coverslips with cells were rinsed in PBS, counterstained and mounted with Fluoroshield mounting medium with DAPI (Cat# ab104139, Abcam, Cambridge, MA, USA).

*Terminal deoxynucleotide transferase mediated dUTP nick-end labelling (TUNEL) assay.* Detection of DNA breakage in nucleus and assessment of apoptosis ratio in the treated cells was determined by Click-iT™ Plus TUNEL assay with Alexa Fluor 488 dye (Cat #C10617, Thermo Fisher Scientific, Waltham, MA, USA). TUNEL staining was performed according to the manufacturer's manual with slightly modifications. Briefly, after permeabilization, cells on coverslips were washed thrice with PBS for 5 min each and incubated in 50 µL of TdT (Terminal deoxynucleotidyl transferase) Reaction Buffer for 10 min at 37 °C. Then TdT Reaction Buffer was removed and 50 µL of freshly prepared TdT reaction mixture containing TdT enzyme and EdUTP in TdT Reaction Buffer were dropped on each coverslip and cells were incubated for 60 minutes at 37 °C in humidified chamber. After that, the coverslips were rinsed in deionized water and washed with blocking serum solution for 5 min. Cover slides were then rinsed in PBS and 50 µl of the Click-iT™ Plus TUNEL reaction cocktail (TUNEL Supermix in TUNEL Reaction Buffer) were added to each coverslip. After 30 min at 37 °C incubation the TUNEL reaction was stopped by removing Click-iT™ Plus TUNEL reaction cocktail and washing coverslips three times for 5 min with blocking serum solution.

*Proliferation assay.* To evaluate cell proliferation rates the TUNEL-stained cells were additionally incubated with primary anti-Ki67 antibodies [SP6], Rabbit monoclonal (1:400 dilution, Cat #ab16667, Abcam, Cambridge, MA, USA) and counterstained with Alexa Fluor 555 Phalloidin (1:500 dilution, Cat #A34055, Thermo Fisher Scientific, Waltham, MA, USA) in blocking serum solution overnight at 4 °C. After washing with PBST for 5 min two times, the secondary donkey anti-rabbit Alexa Fluor 647 antibodies (1:500 dilution, Cat #A-31573, Thermo Fisher Scientific, Waltham, MA, USA) were added and incubated at room temperature for 1h. Cells on coverslips were rinsed in PBS, mounted and counterstained with Fluoroshield mounting medium with DAPI.

*The Confocal Laser Scanning Microscopy.* Images (Figures S13-S15) were acquired using LSM 710 Zeiss confocal microscope (Germany, The Center of Collective Usage «Confocal Microscopy» at the Pavlov Institute of Physiology, Russian Academy of Sciences) equipped with 63x objective. In the microscope, DAPI was excited by 405 nm (diod laser, continuouswave/pulsed), Alexa Fluor 488 dye was excited by 488 nm (Ar-laser), Alexa Fluor 555

Phalloidin was excited by 561 nm (DPSS-laser), and Alexa Fluor 647 was excited by 633 nm (HeNe-laser). Images were acquired in the lsm format and processed with ImageJ for export as tiff files. The number of apoptotic cells present in a cover slide expressed as a percentage of the total number of cells, the so-called apoptotic index (AI), measures an apoptotic state. For the purpose of this study, an activated caspase-3 labeling apoptotic index and TUNEL-labeling apoptotic index were calculated. The Ki67 proliferation index (reflects mitogenic activity rate of cells) was calculated in a similar way: as a number of Ki67-positive cells, expressed as percentage of the total number of cells counted in each case. The number of labeled cells in immunostained cover slides were counted relative to total number of cells in one field of view area.

**Table S1.** Comparative table for solvatochromic MOFs. \*upon the infra-red laser heating (Fig. S6).

Year of publication	MOF	Solvent	Color change time (s)	Endurance (numb. of cycles)	Change color	Ref.
2024	CoBTC	H <sub>2</sub> O/DMF	0.1/0.1*	50	Pink/Purple	This work
2021	{[Ni(pzt) <sub>2</sub> (H <sub>2</sub> O) <sub>2</sub> ](H <sub>2</sub> O)(DMF)} <sub>n</sub>	NH <sub>3</sub>	1200	1	Blue/Pale pink	[18]
		MA	1800		Blue/Light green	
		EA	2100		Blue/Pale blue	
		EDA	3000		Blue/Pink	
2020	[Zn <sub>2</sub> (DPMNI)·(TPDC) <sub>2</sub> ]	Ethanol	-	1	Yellow/Bright yellow	[43]
		MeCN	600/-		Yellow/Dark yellow	
		DMF	600/-		Yellow/Brown	
		DMA	600/-		Yellow/Dark red	
		DEF	600/-		Yellow/Orange	
		DMSO	600/-		Yellow/Dark orange	
2020	[Co <sub>3</sub> OBA <sub>3</sub> PTD(H <sub>2</sub> O) <sub>2</sub> ·2DMA·H <sub>2</sub> O] <sub>n</sub>	CH <sub>2</sub> Cl <sub>2</sub>	60	200	Dark red/Purple	[44]
2019	[Mn <sub>6</sub> (C <sub>42</sub> H <sub>24</sub> O <sub>18</sub> P <sub>3</sub> N <sub>3</sub> ) <sub>2</sub> (H <sub>2</sub> O) <sub>5</sub> ] <sub>n</sub>	Acetone	3600	1	Colorless/Light red	[16]
2019	[Zn <sub>3</sub> (btc) <sub>2</sub> (μ <sub>3</sub> -OH)(DMF)]·H <sub>2</sub> O	Nicotine	60	1	Light yellow/Red	[45]
2019	[Co <sub>2</sub> (dpmndi)(bdc) <sub>2</sub> ]·DMF	DMA	1036800	1	Colorless/Green	[17]
		DMSO			Colorless/Red	
2018	{[Cd <sub>2</sub> L <sub>4</sub> (SO <sub>4</sub> )(H <sub>2</sub> O)]	Benzaldehyd	86400	1	Pale yellow/Bright	[46]

	$\cdot(\text{SO}_4)\cdot 2\text{H}_2\text{O}\}_n$	e			yellow	
2018	$\text{Co}_3[\text{Co}(\text{CN})_6]_2$	Ethanol	60	1	Pink/Purple	[47]
2018	Tb-MOF	EtOH	432000	1	Colorless/Light yellow	[48]
		$\text{CH}_3\text{CN}$			Colorless/Orange	
2017	$[\text{Cd}_2(\text{ipbp})_2(\text{NO}_3)_2]\cdot 2\text{DMF}$	DEA	2400	1	Light yellow/Pink	[49]
2015	$[\text{Cu}(\text{L})(\text{I})_{2n}\cdot 2n\text{DMF}\cdot n\text{MeCN}]$	$\text{H}_2\text{O}$	86400	1	Orange/Brown	[51]
		DMSO	604800		Brown/Orange	
		MeOH	604800		Orange/Brown	
2013	$[(\text{CH}_3)_2\text{NH}_2]_2[\text{ZnNa}_2(\mu_2\text{-H}_2\text{O})_2(\text{H}_2\text{O})_2(\text{TATA T})]\cdot 2\text{DMF}$	Acetone	1800	1	Colorless/Light yellow	[52]
		Ethanol	18000		Colorless/Light yellow	
2011	$\{[(\text{WS}_4\text{Cu}_4)\text{I}_2(\text{dptz})_3]_3\text{DMF}\}_n$	$\text{CH}_3\text{CN}$	60/-	1	Bright red	[50]
		DMF		1	Dark red	
		Acetone		1	Dark red	
		$\text{CHCl}_3$		10	Black	
		$\text{H}_2\text{O}$		1	Red	
		$\text{CH}_3\text{OH}$		10	Dark red	
		$\text{C}_2\text{H}_5\text{OH}$		1	Black	
		$\text{H}_2\text{O}/\text{glycol}/\text{CH}_3\text{CN}$		1	Pale pink	
		$\text{H}_2\text{O}/\text{CH}_3\text{CN}$		1	Blue	



**Table S2.** Crystal data and structure refinement for CoBTC (CCDC 2128895).<sup>32</sup>

Identification code	CoBTC
Empirical formula	C <sub>18</sub> H <sub>32</sub> Co <sub>3</sub> O <sub>24</sub>
Formula weight	809.22
Temperature/K	299.25
Crystal system	monoclinic
Space group	C2
a/Å	17.4650(7)
b/Å	12.9593(6)
c/Å	6.5640(3)
$\alpha$ /°	90
$\beta$ /°	111.9760(10)
$\gamma$ /°	90
Volume/Å <sup>3</sup>	1377.71(11)
Z	2
$\rho_{\text{calc}}$ /g/cm <sup>3</sup>	1.951
$\mu$ /mm <sup>-1</sup>	1.893
F(000)	826.0
Crystal size/mm <sup>3</sup>	0.15 × 0.03 × 0.03
Radiation	MoK $\alpha$ ( $\lambda$ = 0.71073)
2 $\Theta$ range for data collection/°	4.026 to 63.77
Index ranges	-25 ≤ h ≤ 20, -17 ≤ k ≤ 18, -9 ≤ l ≤ 9
Reflections collected	11192
Independent reflections	4009 [R <sub>int</sub> = 0.0220, R <sub>sigma</sub> = 0.0306]
Data/restraints/parameters	4009/1/219
Goodness-of-fit on F <sup>2</sup>	1.051
Final R indexes [I ≥ 2 $\sigma$ (I)]	R <sub>1</sub> = 0.0289, wR <sub>2</sub> = 0.0722
Final R indexes [all data]	R <sub>1</sub> = 0.0312, wR <sub>2</sub> = 0.0736
Largest diff. peak/hole / e Å <sup>-3</sup>	0.85/-0.39
Flack parameter	0.285(5)

## PXRD analysis

In the analysis below, it was initially assumed the samples were single-phase, and the instrumental parameters were calibrated to ensure the as-received structure was fully compliant with the input MOF structure. Given these assumptions, a deviation of the calculated XRD profiles from the experimental data could be indicative to structural transformations occurring after solvent exchange.

The experimental XRD profiles (Figure S1) showed appreciable noise levels, which typically occurs in thin-film samples. Additionally, an amorphous peak was visible in the background (Figures S2-S4). Rietveld refinement in MOF 1 specimen resulted in a good overall fit to the experimental data with no optimization required for the atomic positions in the unit cell (top row of Figures S1a,b). The discrepancy between the experimental and the calculated structures shows up after DMF treatment and fully develops after soaking the MOF in water. To mitigate this discrepancy, partial optimization of the atomic position was applied, as detailed in the Methods section. This results in a much better quality of fit – see Figure S1b. At the same time, when looking at the unit cell parameters listed in Table S4, it becomes clear that the structure does not fully recover after DMF and H<sub>2</sub>O treatment, particularly when looking at the values of *a* and *b* lattice parameters. Concerning the initial hypothesis, the refinement results presented above might be interpreted as an indication of a structural transition where the nearest neighbors of Co atoms are mostly mobile.

### Optimization parameters for PXRD:

#### 1. Residuals after refinement (MOF 2):

wR = 1.867 % - optimized positions

wR = 2.844 % - NO optimization in atomic positions

Reduced  $\chi^2$  = 1.76 (optimized)

Reduced  $\chi^2$  = 4.05 (no optimization)

GOF = 1.33 vs GOF = 2.01

#### 2. Residuals after refinement (MOF 3):

wR = 1.613 %

Reduced  $\chi^2$  = 1.18

GOF = 1.09

**Table S3.** Parameters of PXRD comparative analysis. Positions of peaks: 1 – 17.5  $\Theta$ ; 2 - 17.8  $\Theta$ ; 3 - 18.7  $\Theta$ ; 4 – 21.9  $\Theta$ .

	FWHM				Ratio of peaks			
	1 peak	2 peak	3 peak	4 peak	1/3	2/3	2/4	3/4
MOF 1	0.11	0.12	0.16	0.13	0.81	0.31	0.89	2.85
MOF 2	0.12	0.12	0.16	0.13	1.14	0.41	0.71	1.72
MOF 3	0.13	0.13	0.16	0.14	0.80	0.35	0.88	2.46

**Table S4.** Unit cell parameters determined through Rietveld refinement. An “Atomic positions – preserved” part indicates the expected behaviour (recovery of the parameter following soaking in water), while “Atomic positions – partially optimised” corresponds to progressive deviation from the dry state.

	<i>a</i> (Å)	<i>b</i> (Å)	<i>c</i> (Å)	$\beta$
<i>Atomic positions – preserved</i>				
MOF 1	17.41476	12.95142	6.54728	111.821
MOF 2	17.40585	12.95880	6.54790	111.823
MOF 3	17.41782	12.95085	6.54807	111.838
<i>Atomic positions – partially optimised</i>				
MOF 1	17.41922	12.94896	6.5474	111.851
MOF 2	17.40870	12.95882	6.5475	111.850
MOF 3	17.41899	12.94633	6.5471	111.858

High noise (Figure S2) levels make refinement of atomic position particularly challenging. When conducting unconstrained refinement of all atomic positions, the resulting structures are realistic (Figure S3). Partial optimization of just the Co atoms and their nearest neighbors produce similar quality of fit. At the same time, the structures tend to be more realistic. It should be noted that the structure below could only serve as schematic representations of the changes occurring in the real material. Under such high noise levels, accurate quantification of atomic positions is impossible.

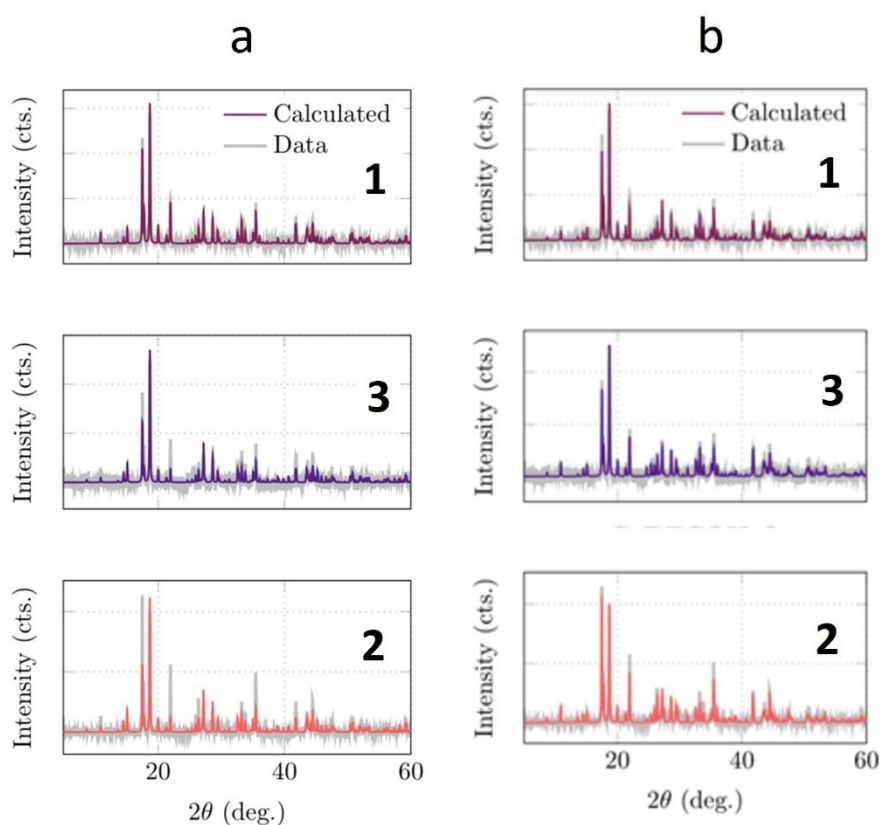


**Figure S1.** Full-profile Rietveld refinement of experimental XRD profiles in the MOF prior to any treatment (MOF **1**), after being exposed to DMF (MOF **3**) and subsequently to water (MOF **2**): (a) refinement first took place without optimising the atomic positions; (b) positions of nearest neighbors of Co atoms were finely tuned. The background-subtracted raw data is shown in grey whilst the thick colored lines correspond to the calculated profiles. The results are consequences of Figures S2-S4 summary up.

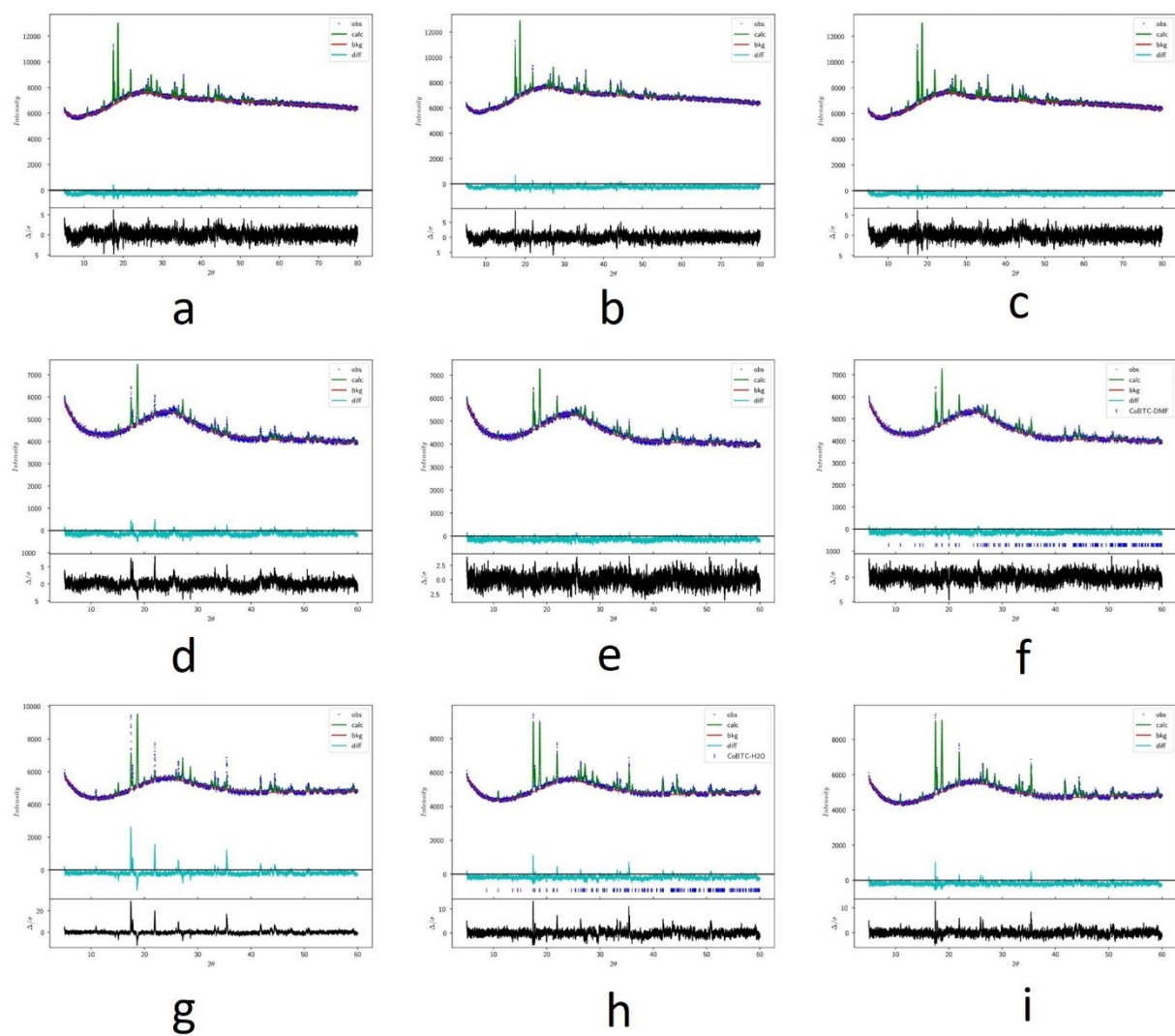


**Figure S2.** Rietveld refinement of MOF 1 (a-c), MOF 3 (d-f), and MOF 2 (g-i). Atomic positions were not optimized in (a,d,g), only Co atoms and nearest neighbors were optimized in (b,e,h). Full atomic optimization was conducted in (c,f,i).

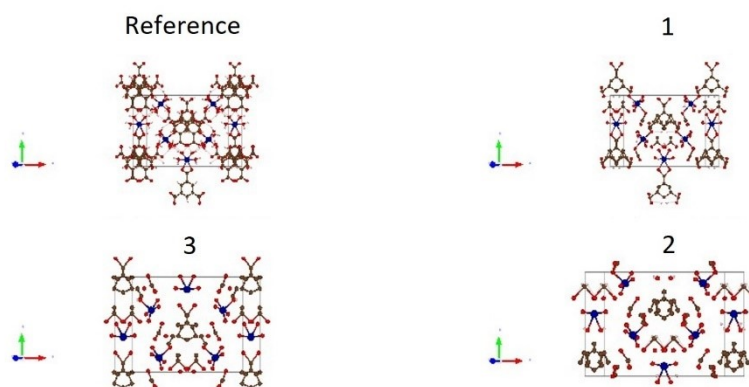


**Figure S3.** Candidate structures after optimization of all atomic positions.

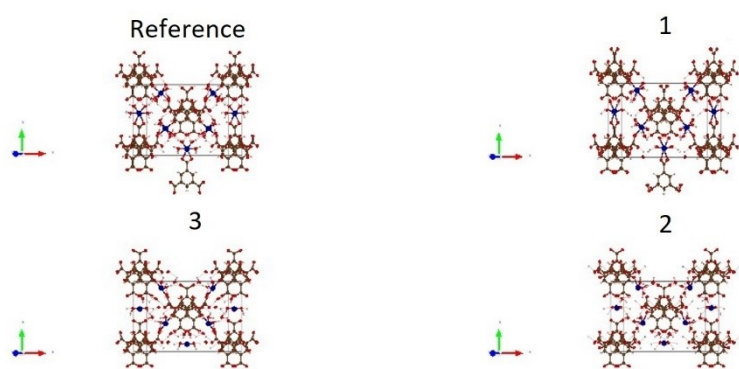


**Figure S4.** Candidate structures after optimization of Co atoms and nearest neighbors.

### Computational Details and Optics

The density-of-states and HOMO-LUMO energy levels for model system based on the experimental X-ray geometry have been calculated with DFT using the dispersion-corrected hybrid functional  $\omega$ B97XD<sup>53</sup> with the help of Gaussian-09 program package<sup>54</sup> and Multiwfn program (version 3.7).<sup>55</sup> The 6-311+G\* basis sets were used for all atoms. The solvent effect has been taken into account using the SMD (Solvation Model based on Density) continuum solvation model suggested by Truhlar and coworkers.<sup>56</sup> The calculated energies are presented in Table S5.

**Table S5.** Energy levels of highest occupied and lowest unoccupied molecular orbitals (HOMO and LUMO, in eV) in MOF 2 and MOF 3.

Model system	HOMO <sub><math>\alpha</math></sub>	LUMO <sub><math>\alpha</math></sub>	HOMO <sub><math>\beta</math></sub>	LUMO <sub><math>\beta</math></sub>
MOF 3	-7.88	-5.19	-7.56	-5.04
MOF 2	-8.91	-3.22	-8.87	-4.99

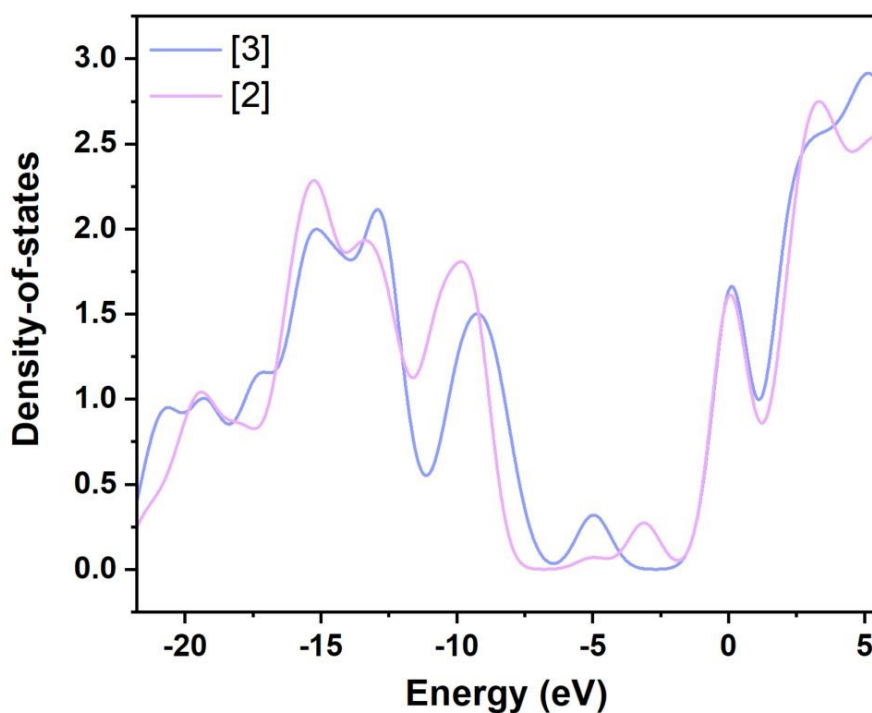


**Figure S5.** Density-of-states for MOF 2 and MOF 3.

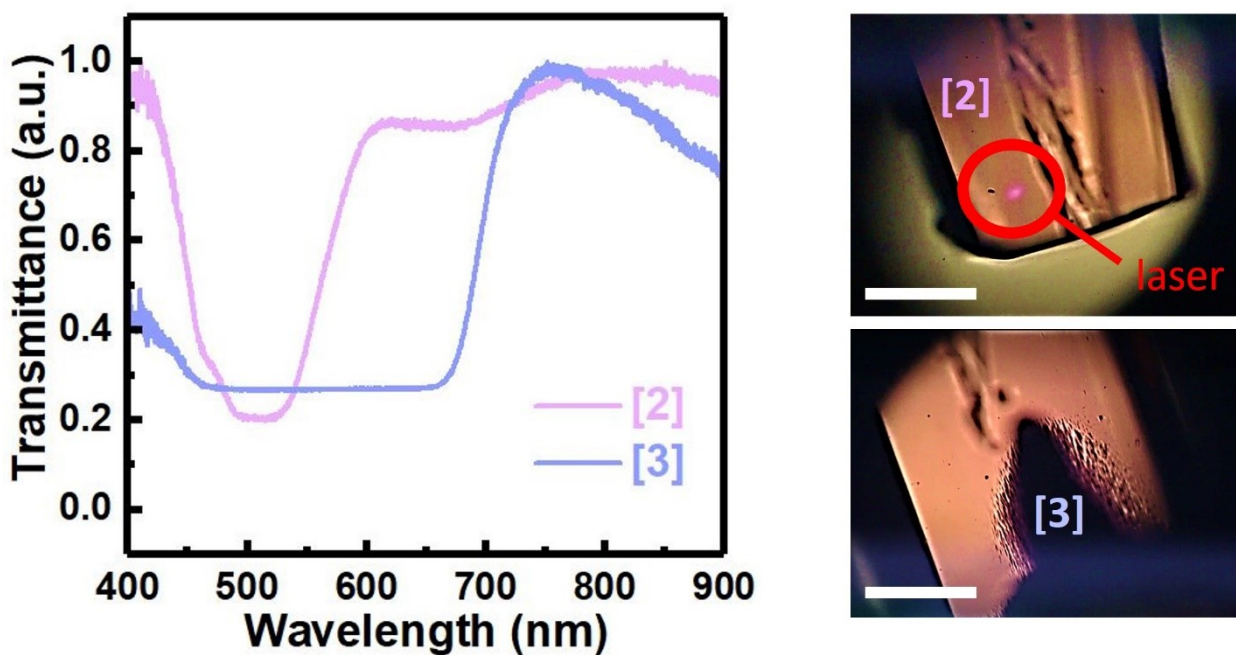


**Figure S6.** (left) Normalized optical transmittance spectra for the single crystal of MOF **2** (pink curve) and MOF **3** (purple curve) during the infra-red laser heating (see Material and Methods), initiated by solvent exchange. (right) Optical images of MOF **2** (before laser heating, [2]) converting into MOF **3** by laser heating ([3]).

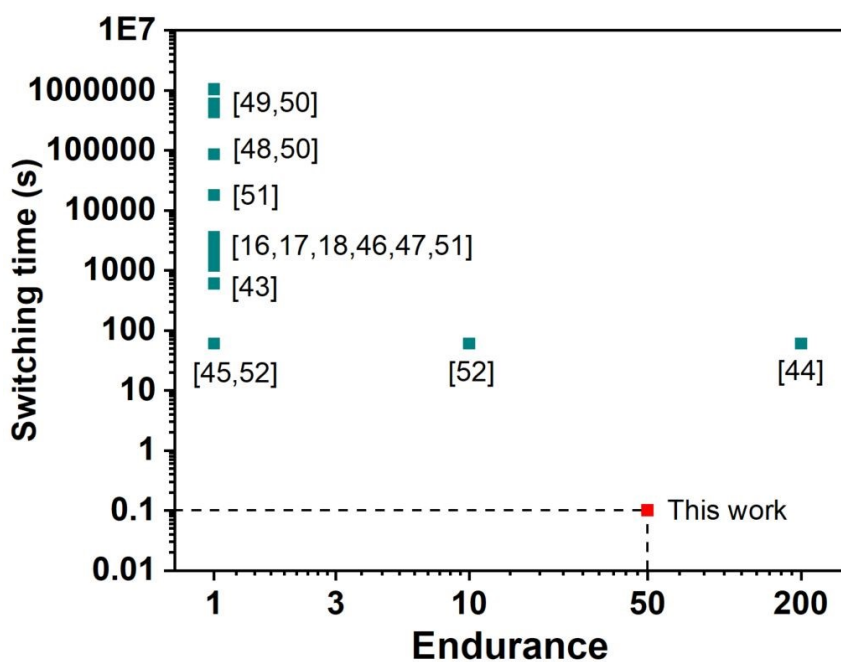


**Figure S7.** Diagram of the color change time vs endurance of solvatochromism of existing MOFs compared with our results (Fig. 3h).



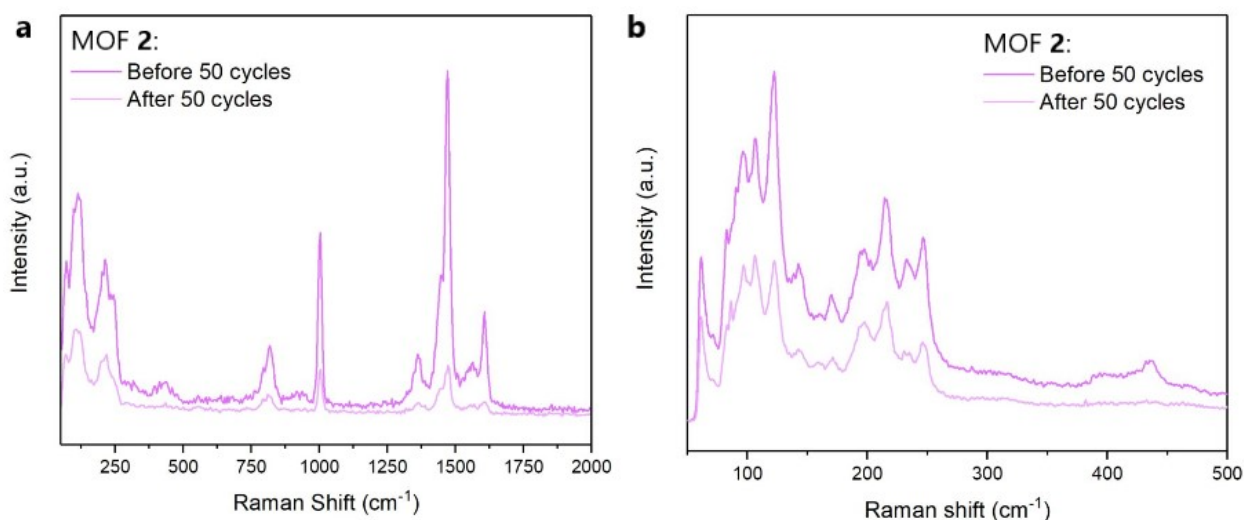


**Figure S8.** (a) Raman spectra for the powder of MOF 2 before and after 50 cycles of solvent exchange (H<sub>2</sub>O/DMF). (b) The spectral region 50-500 cm<sup>-1</sup>, detected with a 1800 g mm<sup>-1</sup> diffraction grating for detailed description of the region of coordination bonds and low-energy phonons.

**Table S6.** Raman peak assessment for MOF 1, MOF 2 and MOF 3.

MOF 1	MOF 2	MOF 3		
Peak position, cm <sup>-1</sup>	Peak position, cm <sup>-1</sup>	Peak position, cm <sup>-1</sup>	Assignment of Bonds	Ref.
90 - 250			Low-energy phonons of the periodic lattice of MOF	[60-62]
411	439	411	Co-O coordination bond	[57]
660		660	O=C-N in-plane bending of DMF	[34,35]
826	826	826	C-H	[58]
875		878	stretching of the C-N and (CH <sub>3</sub> )N bond of DMF	[34,35]
1015	1015	1015	C=C	[58]
1100		1100	stretching of the C-N and (CH <sub>3</sub> )N bond of DMF	[34,35]
1400-1600			C-C, C-O <sub>2</sub> , and C=C	[57,58]
1666		1666	reflecting the vibration of C=O bond of DMF	[34,35]

## Biocompatibility

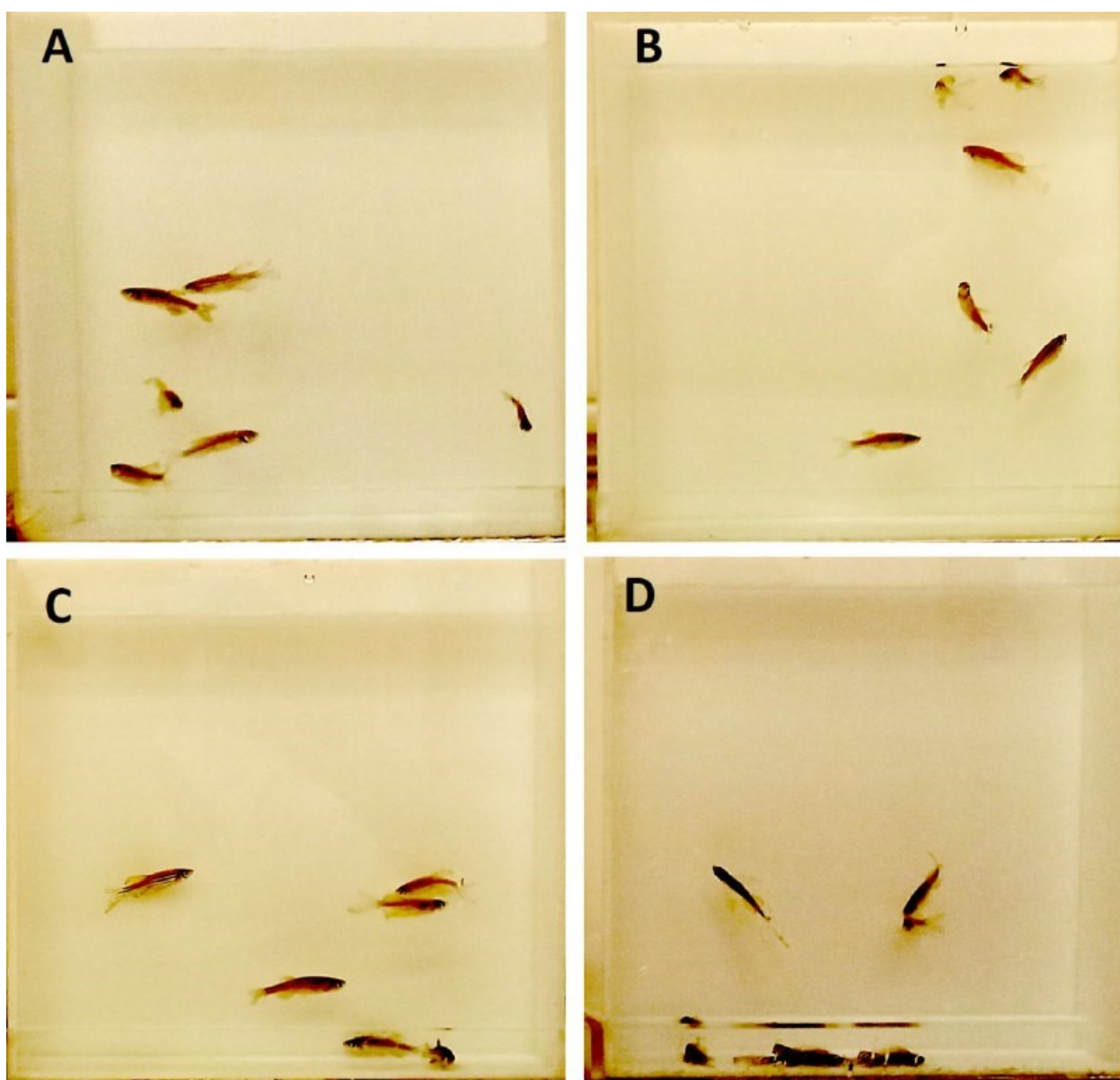


**Figure S9.** Behavioral test showed different reactions of fish in 3 hours after intragastric injection of the MOF 2: (A) At a dose of  $1.5 \text{ g kg}^{-1}$  (equal to 1.5 g of the MOF powder to 1 kg of fish), the fish stayed closer to the center of the chamber, demonstrating healthy behavior; (B-D) while the injection of higher dose (3 to  $12 \text{ g kg}^{-1}$ ) led to changes in behavior relative to the first group. (B) At a dose of  $3 \text{ g kg}^{-1}$ , some fish began to gasp for air from the surface, (C) while at a dose of  $6 \text{ g kg}^{-1}$ , 2 fish out of 6 began to lie motionless on the bottom of the chamber. (D) When the dose was  $12 \text{ g kg}^{-1}$ , only 2 fish out of 6 continued to swim.

Toxicity study was also performed for MOF 3 powder using four groups of wild-type fish with 6 individuals each, the age of the zebrafish was 6 months, the average weight was 330 mg. Using a micro-dispenser, we introduced an aqueous suspension of MOF 3 particles into the stomach of

fish. Suspensions were prepared in the E3 medium at four concentrations: 200, 100, 50 and 25 mg/ml. These volumes of suspensions corresponded to dosages of 12.0, 6.0, 3.0, and 1.5 g kg<sup>-1</sup> of fish weight. To introduce the suspension into the stomach, we immobilized the fish by incubating them in a 170 mg l<sup>-1</sup> tricaine solution for 5 min, after MOFs injection we placed the fish in an aquarium with running water. Three hours after the introduction of particles into the stomach, we placed each group of fish in a behavioral chamber and took photographs. We took repeat photographs 6 hours after the introduction of particles.

Adult zebrafish mortality as toxicity endpoint was assessed after the introduction of the suspension into the stomach after 6 hours (Figure S10). At this time interval, a behavioral test is conducted, and we assessed the distribution of fish in behavioral chambers. The toxic effect on fish behavior included anxiety, depressed behavior, and the position the fish occupied in the aquarium.

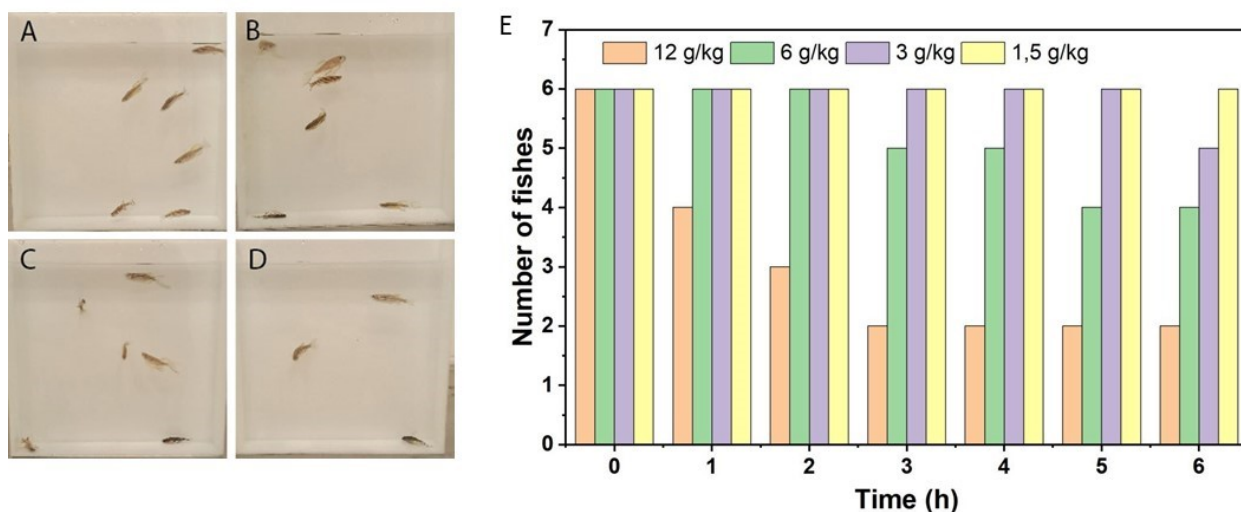


**Figure S10.** Behavioral response of zebrafish to intragastric injection of different doses of the MOF 3 after 6 h: (a) 1.5 g kg<sup>-1</sup> – float throughout the entire volume; (b) 3 g kg<sup>-1</sup> – death of one, the rest float throughout the entire volume; (c) 6 g kg<sup>-1</sup> – death of two, the rest float throughout the entire volume; (d) 12 g kg<sup>-1</sup> – 2 fish remain alive; (e) Adult zebrafish survival test to intragastric MOF 3 injection: Injection of different doses of MOF 3 from 1.5 to 12 g kg<sup>-1</sup> resulted in different levels of fish survival within 6 h.

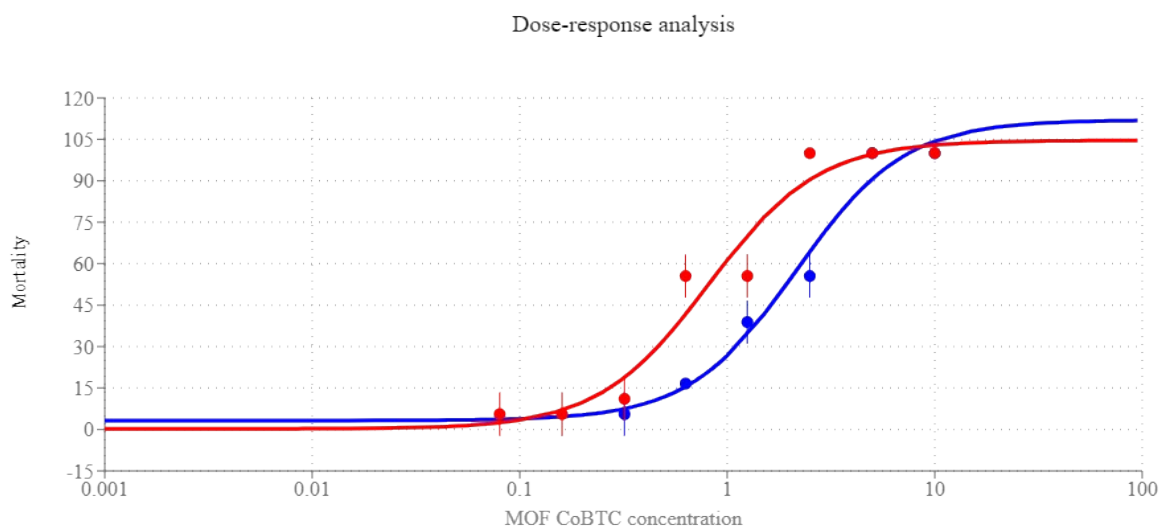


**Figure S11.** Graphs of embryo mortality versus the MOF **2** concentration, 24 h (blue) and 72 h (red).

T98G cell viability test was performed (see Materials and Methods). Figure S12 demonstrates cell viability after the exposure of different concentrations of the MOF **2** (15.625 to 2000  $\mu\text{g mL}^{-1}$ ) studied for 6, 18, and 24 h. Both dose-dependent and time-dependent effects were observed (Figure S12a). At a low concentration of MOFs (up to 31.25  $\mu\text{g mL}^{-1}$ ) during three time points, low cytotoxicity was revealed (cell viability is over 70 %). From the cell viability results, we also calculated the IC<sub>50</sub> (50 % growth inhibition) at 6, 18, and 24 h (for 62.49 to 89.88  $\mu\text{g mL}^{-1}$  concentration, Figure S12b). Microscopic study of the T98G cells showed changes in their morphology and decreased cell density at the concentration of the MOF over 31.25  $\mu\text{g mL}^{-1}$  (Figures S13a, S14a, S15a). Thus, we chose sub-toxic (31.25  $\mu\text{g mL}^{-1}$ , cell viability 72–92%) and toxic (250 and 1000  $\mu\text{g mL}^{-1}$ , viability 3.6–18.5 %) doses of the MOF **2** to assess the morphological features, effect on cell proliferation and apoptosis induction (2 mM DTT solution was used as positive control of apoptosis induction). Concerning the apoptotic activity, at a low concentration of the MOF, the corresponding low apoptotic index values were detected. Regardless of the incubation time (6, 18, or 24 h), no statistically significant difference was observed between intact cells and cells incubated with the MOF at a subtoxic concentration of 31.24  $\mu\text{g mL}^{-1}$ . Herein, the number of cells stained with antibodies to activated caspase3 when exposed to the MOF **2** for 6, 18, and 24 h at the concentration of 250 and 1000  $\mu\text{g mL}^{-1}$  was statistically different from the negative control (0  $\mu\text{g mL}^{-1}$ ,  $p < 0.001$ , see Figure S13a,b).

Next, to investigate the MOFs ability to induce apoptosis in T98G cells, terminal deoxynucleotidyl transferase (TdT) dUTP Nick-End Labeling (TUNEL) assay was performed after 6, 18 and 24 h of incubation. The lowest TUNEL-labeling apoptotic index was observed in cells incubated with 31.25  $\mu\text{g mL}^{-1}$  of the MOF during all time intervals (Figure S14a,b). There was no difference in

apoptotic index between the control (cell culture medium at 0  $\mu\text{g mL}^{-1}$  of the MOF) and 31.25  $\mu\text{g mL}^{-1}$  of the MOF exposed groups at 6 hours, while apoptotic index significantly increased after 18 and 24 h of incubation. With increasing concentration of the MOF, a tendency to increase the number of TUNEL-positive apoptotic cells was observed; however, at 6 and 24 h of incubation, the apoptotic index was not statistically different between the 31.25, 250, and 1000  $\mu\text{g mL}^{-1}$  groups. After 18 h of incubation, no difference in apoptotic index was observed between cells incubated with 250 and 1000  $\mu\text{g mL}^{-1}$  concentration of the MOF **2**.

Immunohistochemical staining of T98G cells for the proliferation marker Ki67 revealed no statistically significant differences between the control group (0  $\mu\text{g mL}^{-1}$ ) and cells treated with 31.25 and 250  $\mu\text{g mL}^{-1}$  of the MOF for 6 h. Increase in the MOF concentration resulted in a statistically significant decrease in proliferative activity (number of Ki67 positive cells), compared with the positive control (at 2 mM DTT) at all time points (see Figure S15a,b). Furthermore, morphological changes were observed in the cells treated with the MOF **2**. The cells changed their morphology as the concentration of the MOF in the solution and the incubation time increased: At a subtoxic concentration (31.25  $\mu\text{g mL}^{-1}$ ), the cells were predominantly attached and spread out on the substrate (in 6 h). As the incubation time increased (18 and 24 h), individual rounded cells of reduced size appeared, and few cells were stained with antibodies to activated caspase3 (Figure S13a), and also demonstrated DNA damage (TUNEL-positive cells, Figure S14a). Higher MOF concentrations led to morphological changes in the cells already after incubation for 6 h, the proportion of cells positive for caspase3 (Figure S13b) and TUNEL (Figure S14b) increased.

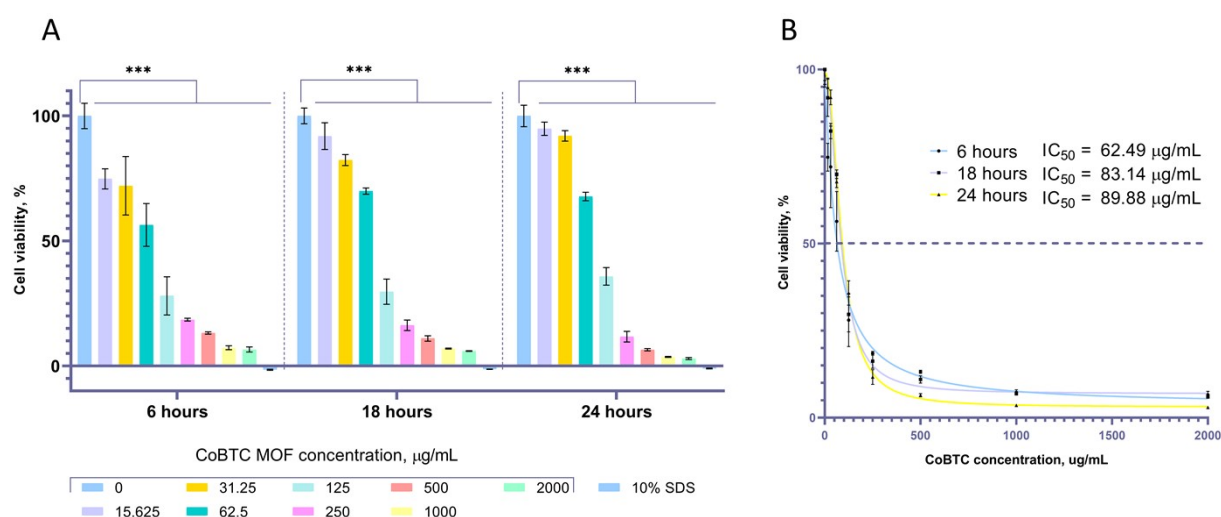


**Figure S12.** MOF **2** effect on cell viability. (A) Comparison of T98G cells exposed to different concentrations of the MOF **2** after 6, 18, and 24 h of incubation. Mean values  $\pm$  standard deviation of six biological replicates. Statistical analysis was performed by one-way ANOVA followed by Dunnett's multiple comparisons test, \*\*\* $p < 0.001$ ,  $n = 6$ . (B) IC<sub>50</sub> values were calculated from



the curves of cell viability after 6, 18, and 24 h incubation. All the values are average of replicates expressed relative to cell viability values in control cells normalized to 100 %. Data points represent average of six technical replicates per MOF' concentration for each experiment  $\pm$  SD.

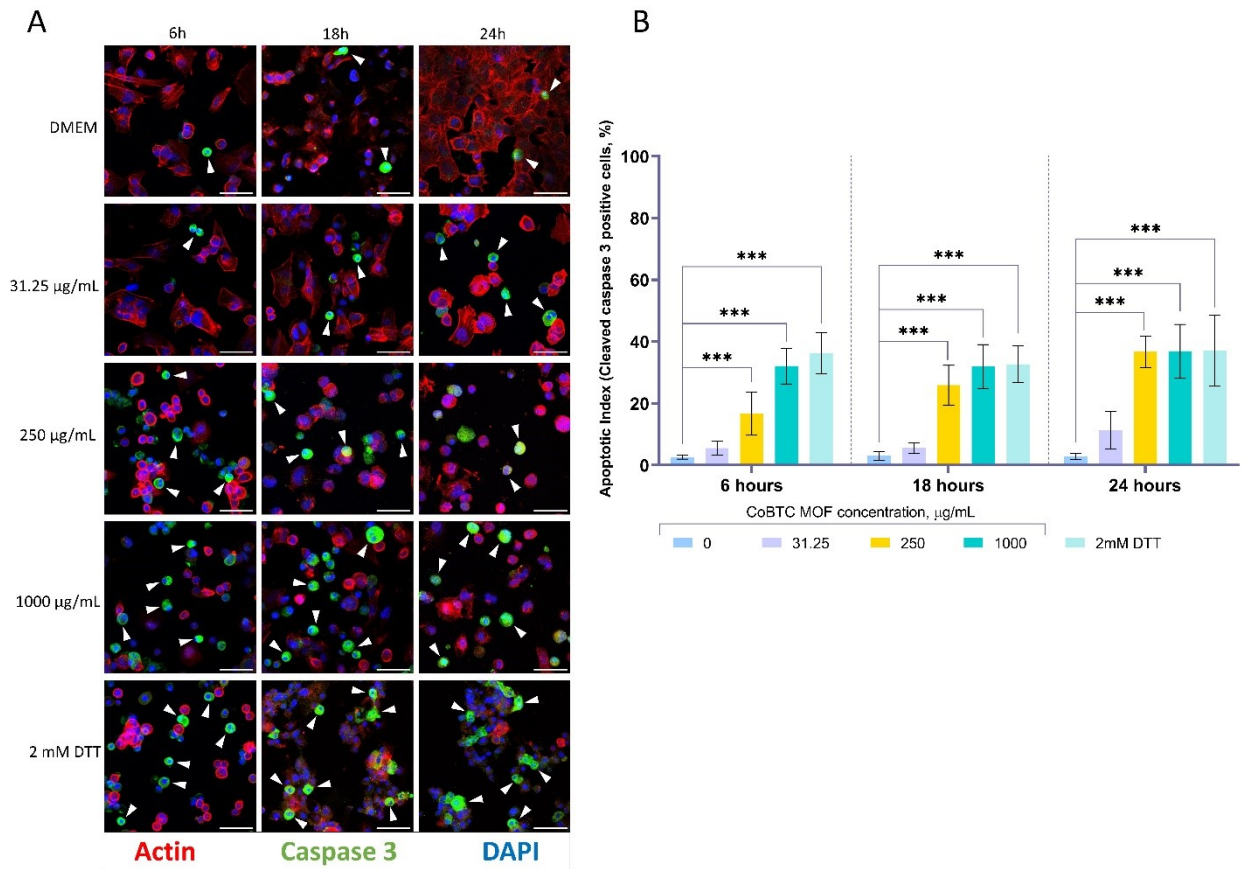


**Figure S13.** MOF 2 ability to induce caspase 3 activation. (A) Caspase3 activation is detected as localization of green signal in cell cytoplasm (white arrows). Scale bars, 50  $\mu$ m. (B) The percentage of cleaved caspase3 positive cells was calculated and shown as graphs. Statistical analysis was performed by one-way ANOVA followed by Dunnett's multiple comparisons test. Results were represented as mean  $\pm$  SD. \*\*\* $p < 0.001$ ,  $n = 6$ .

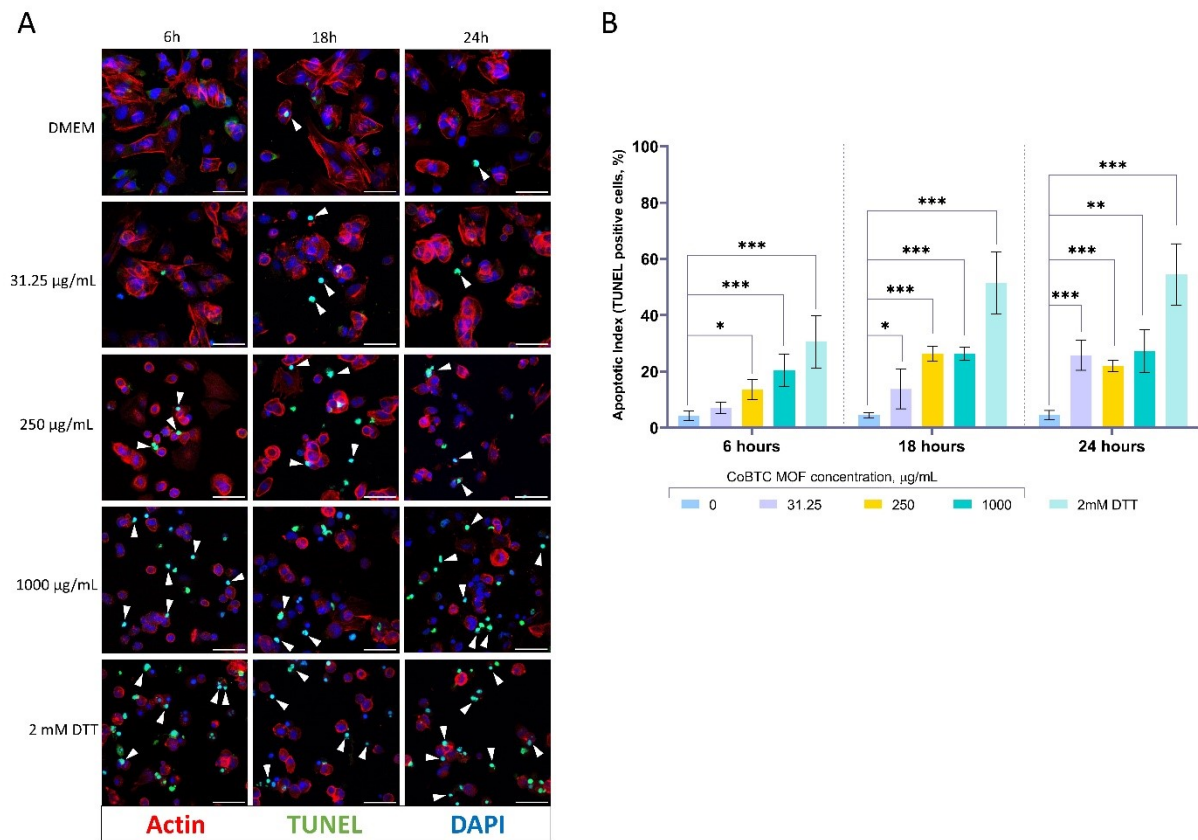


**Figure S14.** MOF 2 ability to induce apoptotic DNA fragmentation. (A) DNA fragmentation is detected as co-localization of green (TUNEL) and blue (DAPI) signals (white arrows). Scale bars, 50  $\mu\text{m}$ . (B) The percentage of TUNEL-positive cells was calculated and shown as graphs. Statistical analysis was performed by one-way ANOVA followed by Dunnett's multiple comparisons test. Results were represented as mean  $\pm$  SD. \* $p < 0.05$ , \*\* $p < 0.005$ , \*\*\* $p < 0.001$ ,  $n = 6$ .

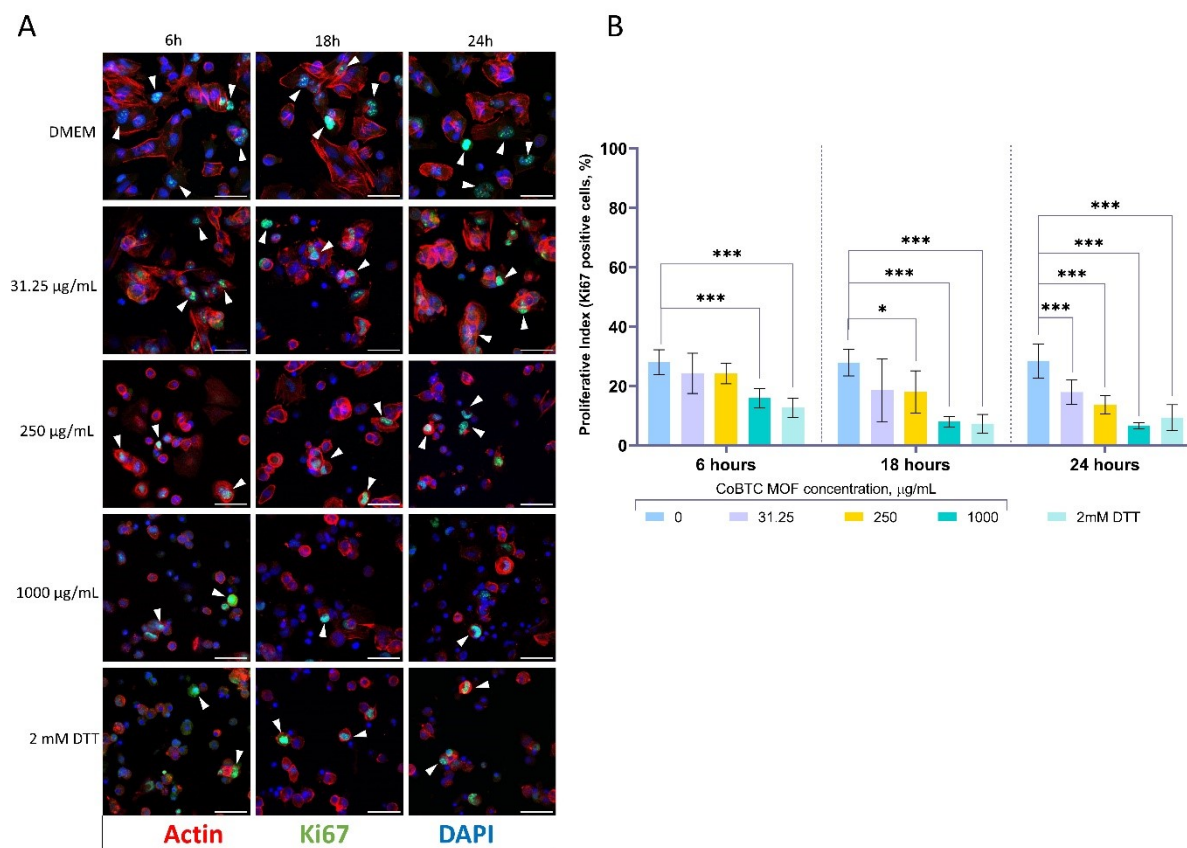


**Figure S15.** MOF 2 effect on cell proliferation. (A) Proliferative activity is detected as co-localization of green (Ki67) and blue (DAPI) signals (white arrows). Scale bars, 50 µm. (B) The percentage of Ki67 positive cells was calculated and shown as graphs. Statistical analysis was performed by one-way ANOVA followed by Dunnett's multiple comparisons test. Results were represented as mean ± SD. \* $p < 0.05$ , \*\*\* $p < 0.001$ ,  $n = 6$ .



## BET analysis

The N<sub>2</sub> adsorption–desorption isotherms of MOF is presented in Figure S16. According to the IUPAC classification, the obtained adsorption–desorption isotherms can be referred to type II with the hysteresis loop corresponding to type C (wedge shaped pores).<sup>59</sup> The BET specific surface area was calculated as 25 m<sup>2</sup> g<sup>-1</sup>. The pore size of material was about 2.897 nm. At the same time, there exist a small number of pores at 4.5 nm and 6.2 nm, probably formed by stacking owing to the incomplete crystallization.

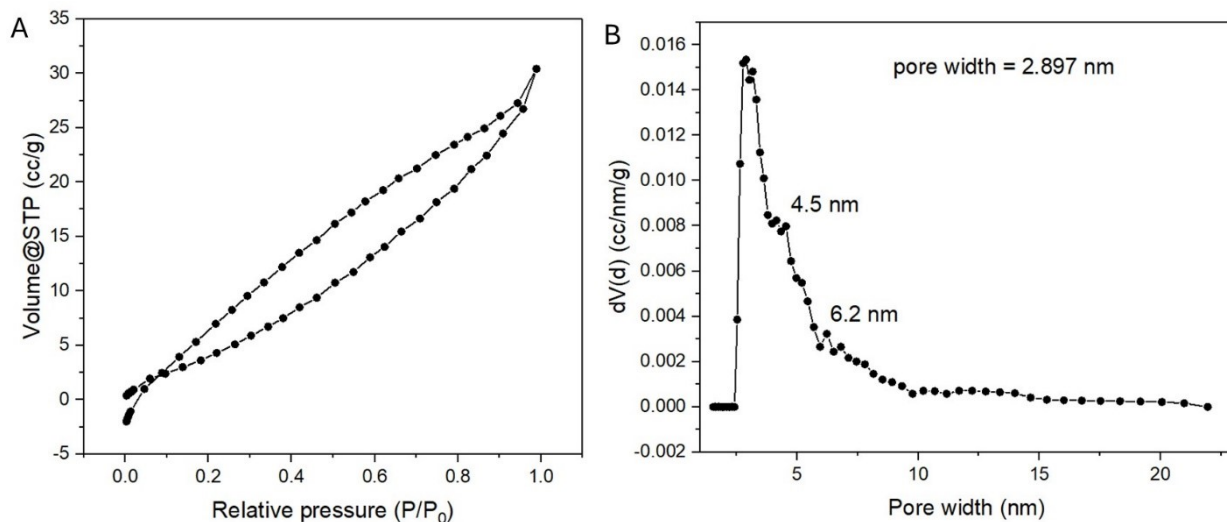


**Figure S16.** (a) N<sub>2</sub> sorption isotherms of MOF at 77 K and (b) pore size distribution simulated by NLDFT model.

## Solvatochromism

The solvent selectivity of solvatochromic MOFs definitely comes from multiple factors like (and not limited to) specific surface area of MOFs, degree of porosity and crystallinity, specific pore shape, their size and structure, abundance of active sites, viscosity of solvents, temperature and pressure regime of the experiment.<sup>63-65</sup> Therefore, this question on the nature of selective solvatochromism of MOFs remains open for the coordination chemistry of functional materials.<sup>66</sup>

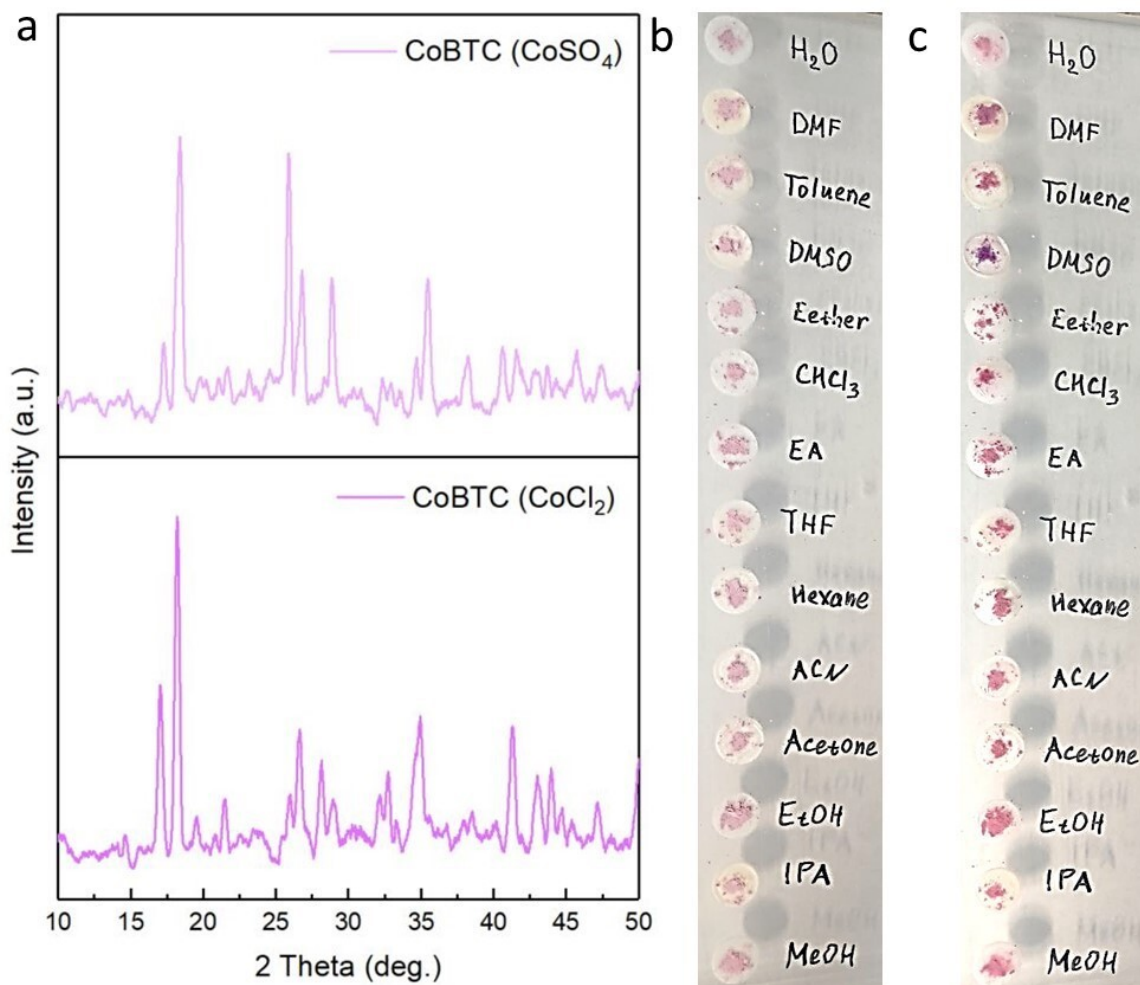


**Figure S17.** (a) The powder X-Ray diffraction pattern of the as-synthesized MOFs (CoBTC) based on initial sulfate or chloride cobalt salts. (b,c) Sensitivity test of the MOFs based on sulfate cobalt salt to different solvents (H<sub>2</sub>O, DMF, Toluene, DMSO (Dimethyl sulfoxide), Ether, CHCl<sub>3</sub>, EA (Ethyl acetate), THF (Tetrahydrofuran), Hexane, ACN (acetonitrile), Acetone, EtOH, IPA (Isopropyl Alcohol), and MeOH) before the solvent exchange (b), and after (c).

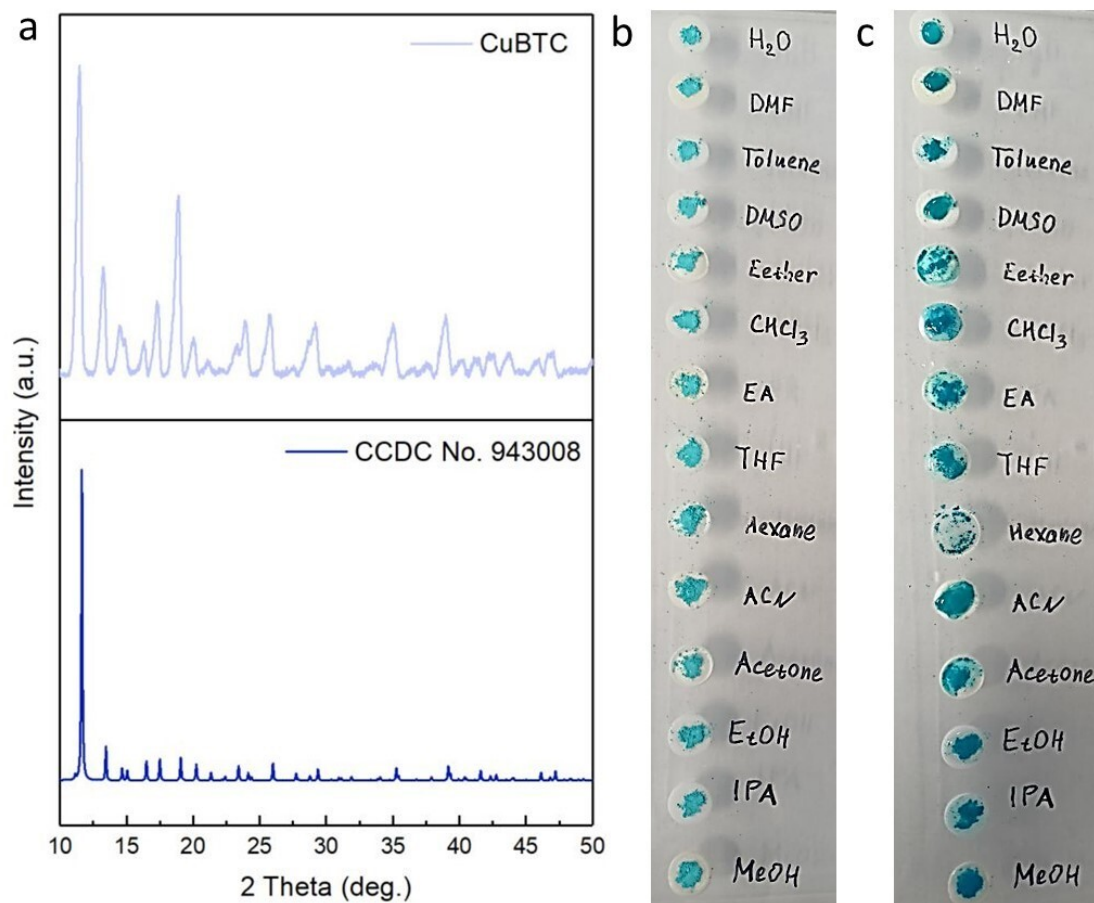


**Figure S18.** (a) The powder X-Ray diffraction pattern of the as-synthesized and stimulated MOFs (CuBTC) based on  $\text{CuCl}_2 \cdot 2\text{H}_2\text{O}$  salt. (b,c) Sensitivity test of the MOF to different solvents ( $\text{H}_2\text{O}$ , DMF, Toluene, DMSO (Dimethyl sulfoxide), Ether,  $\text{CHCl}_3$ , EA (Ethyl acetate), THF (Tetrahydrofuran), Hexane, ACN (acetonitrile), Acetone, EtOH, IPA (Isopropyl Alcohol), and MeOH) before the solvent exchange (b), and after (c).

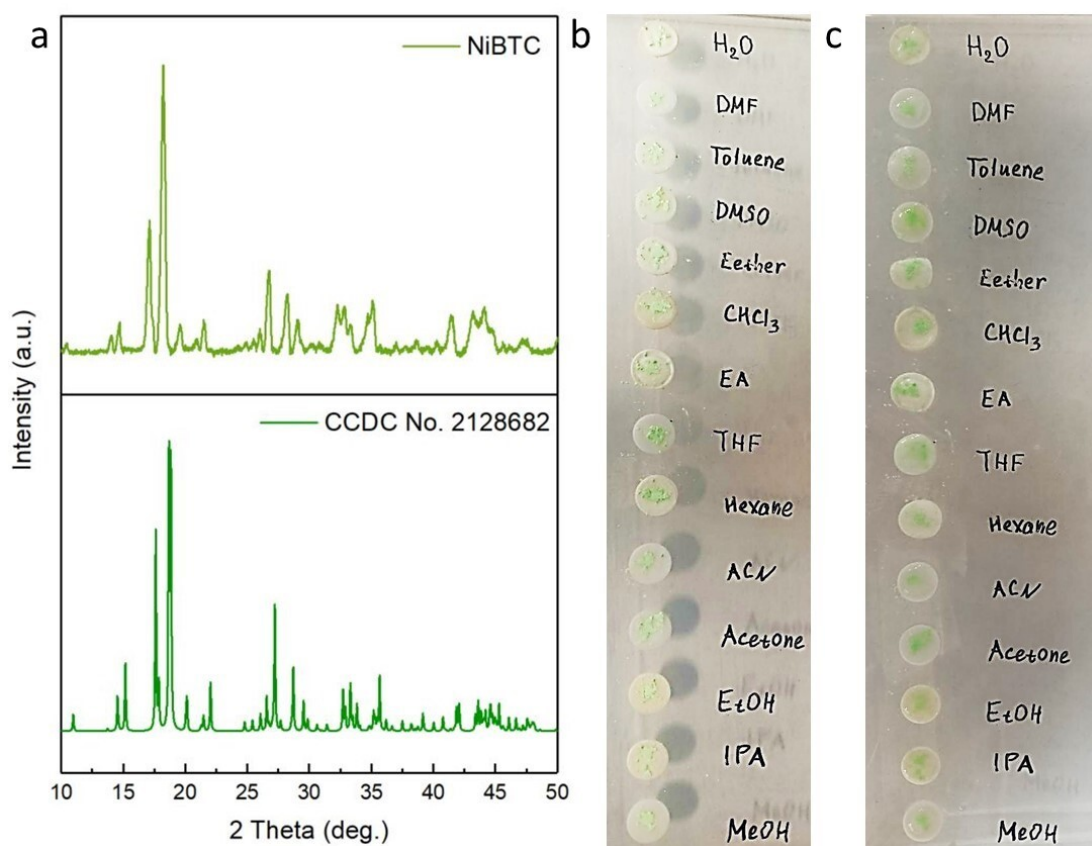


**Figure S19.** (a) The powder X-Ray diffraction pattern of the as-synthesized and stimulated MOF (NiBTC) based on  $\text{NiCl}_2 \cdot 6\text{H}_2\text{O}$  salt. (b,c) Sensitivity test of the MOF to different solvents ( $\text{H}_2\text{O}$ , DMF, Toluene, DMSO (Dimethyl sulfoxide), Ether,  $\text{CHCl}_3$ , EA (Ethyl acetate), THF (Tetrahydrofuran), Hexane, ACN (acetonitrile), Acetone, EtOH, IPA (Isopropyl Alcohol), and MeOH) before the solvent exchange (b), and after (c).



**Figure S20.** Sensitivity test of the initial salt  $\text{CoCl}_2 \cdot 6\text{H}_2\text{O}$  (pink color) to different solvents ( $\text{H}_2\text{O}$ , DMF, Toluene, DMSO (Dimethyl sulfoxide), Ether,  $\text{CHCl}_3$ , EA (Ethyl acetate), THF (Tetrahydrofuran), Hexane, ACN (acetonitrile), Acetone, EtOH, IPA (Isopropyl Alcohol), and MeOH) after the solvent exchange.

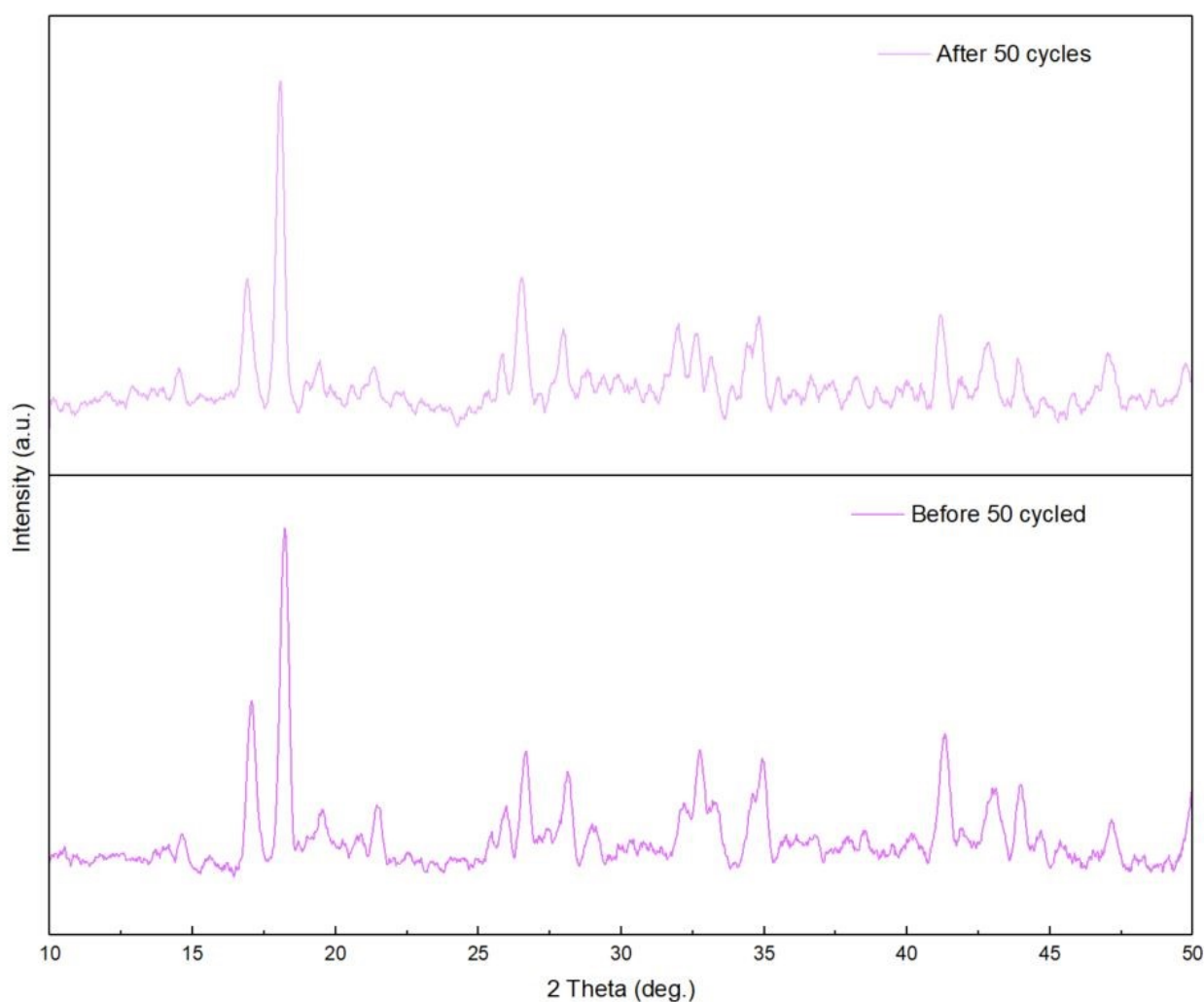


**Figure S21.** PXRD for the MOF 2 powder before and after 50 cycles of the solvent H<sub>2</sub>O/DMF exchange.

## References

43. J.-J. Liu, S.-B. Xia, D. Liu, J. Hou, H. Suo, F.-X. Cheng, *Dyes Pigm.* 2020, **177**, 108269.
44. B. Qin, S. Wu, G. Gahungu, H. Li, Y. Zhao, X. Zhang, J. Zhang, *Chem. A Eu. J.* 2020, **26**, 14187–14193.
45. D. Rani, K. K. Bhasin and M. Singh, *ACS Materials Lett.*, 2020, **2**, 9–14.
46. A. Dey, A. Garai, V. Gude, K. Biradha, *Cryst. Growth Des.* 2018, **18**, 6070–6077.
47. Z. Wang, Q. Chen, *Spectrochim. Acta Part A: Mol. Biomol. Spectroscopy* 2018, **194**, 158–162.
48. Z. Cui, X. Zhang, S. Liu, L. Zhou, W. Li, J. Zhang, *Inorg. Chem.* 2018, **57**, 11463–11473.
49. C. Zhang, L. Sun, Y. Yan, Y. Liu, Z. Liang, Y. Liu, J. Li, *J. Mater. Chem. C* 2017, **5**, 2084–2089.
50. M.-D. Zhang, H.-G. Zheng, Z.-Z. Lu and X.-Q. Yao, *CrystEngComm*, 2013, **15**, 9265–9275.
51. S. Khatua, S. Goswami, S. Biswas, K. Tomar, H. Sekhar Jena, S. Konar, *Chem. Mater.* 2015, **27**, 5349–5360.
52. C.-Y. Sun, X.-L. Wang, C. Qin, J.-L. Jin, Z.-M. Su, P. Huang, K.-Z. Shao, *Chem. A Eu. J.* 2013, **19**, 3639–3645.
53. J. D. Chai, M. Head-Gordon, *Phys. Chem. Chem. Phys.* 2008, **10**, 6615–6620.

54. M. J. Frisch, gaussian 09, Gaussian. Inc., Wallingford CT, 2009, **121**, 150-166.
55. T. Lu, F. Chen, *J. Comp. Chem.* 2012, **33**, 580–592.
56. A. V. Marenich, C. J. Cramer, D. G. Truhlar, *J. Phys. Chem. B* 2009, **113**, 6378–6396.
57. R. Kaur, M. Chhibber, P. Mahata and S. K. Mittal, *ChemistrySelect*, 2018, 3, 3417–3425.
58. R. Nivetha, A. Sajeev, A. M. Paul, K. Gothandapani, S. Gnanasekar, P. Bhardwaj, G. Jacob, R. Sellappan, V. Raghavan, K. C. N, S. Pitchaimuthu, S. K. Jeong and A. N. Grace, *Mater. Res. Express*, 2020, 7, 114001.
59. M. M. Labani, R. Rezaee, A. Saeedi and A. A. Hinai, *Journal of Petroleum Science and Engineering*, 2013, 112, 7–16.
60. Yuliya A. Kenzhebayeva, Nikita K. Kulachenkov, Sergey S. Rzhhevskiy, Pavel A. Slepukhin, Vladimir V. Shilovskikh, Anastasiia Efimova, Pavel Alekseevskiy, Gennady Y. Gor, Alina Emelianova, Sergei Shipilovskikh, Irina D. Yushina, Alexander Krylov, Dmitry I. Pavlov, Vladimir P. Fedin, Andrei S. Potapov, Valentin A. Milichko. *Commun. Mater.* 2024, 5, 48.
61. Alexander E. J. Hoffman, Irena Senkovska, Leila Abylgazina, Volodymyr Bon, Veronika Grzimek, Anna Maria Dominic, Margarita Russina, Marvin A. Kraft, Inez Weidinger, Wolfgang G. Zeier, Veronique Van Speybroeck, Stefan Kaskel. *J. Mater. Chem. A*, 2023, 11, 15286-15300.
62. Tae Wu Kim, Sunhong Jun, Yoonhoo Ha, Rajesh K. Yadav, Abhishek Kumar, Chung-Yul Yoo, Inhwan Oh, Hyung-Kyu Lim, Jae Won Shin, Ryong Ryoo, Hyungjun Kim, Jeongho Kim, Jin-Ook Baeg, Hyotcherl Ihee. *Nature Commun.* 2019, 10, 1873.
63. G. Mehlana, S. A. Bourne and G. Ramon, *Dalton Trans.*, 2012, 41, 4224.
64. C. N. Dzesse T, E. N. Nfor and S. A. Bourne, *Crystal Growth & Design*, 2018, 18, 416–423.
65. L. Qin, H. Ma, M. Lv, Y. Zhou and L. Han, *Journal of Solid State Chemistry*, 2023, 317, 123660.
  
66. B. Siu, A. R. Chowdhury, Z. Yan, S. M. Humphrey and T. Hutter, *Coordination Chemistry Reviews*, 2023, 485, 215119.